Heliyon 8 (2022) e10017

Contents lists available at ScienceDirect

Heliyon

journal homepage: www.cell.com/heliyon

Research article

Synthetic jets as a flow control device for performance enhancement of vertical axis hydrokinetic turbines: A 3D computational study

Nicolas Botero [a], Nicolas Ratkovich [b], Santiago Lain [c], Omar D. Lopez Mejia [a,*]

[a] Computational Mechanics Research Group, Department of Mechanical Engineering. Universidad de los Andes, Cra 1 Este # 19 A 40, 111711, Bogotá, Colombia
[b] Department of Chemical and Food Engineering, Universidad de Los Andes, Cra 1 Este # 19 A 40, 111711, Bogotá, Colombia
[c] PAI+ Group, Energetics & Mechanics Department, Faculty of Engineering, Universidad Autónoma de Occidente, 760030, Cali, Colombia

ARTICLE INFO

Keywords:
Hydrokinetic turbine
Vertical axis water turbine
Synthetic jets
Flow control
Computational fluid dynamics

ABSTRACT

In the present work, a vertical axis turbine with straight blades was analyzed through a numerical simulation in three dimensions, the performance of the turbine was studied while synthetic jets were used as an active flow control method. To carry out the simulations, the Unsteady Reynolds Averaged Navier-Stokes (URANS) equations were solved on Star CCM+, through the k-ω SST turbulence model. The dynamics of the turbine movement were described using the Overset Mesh technique, capturing the transient characteristics of the flow field. Hydrodynamic coefficients and vorticity fields were obtained to describe the flow behaviour, and the results were compared with two-dimensional simulations of the same system. Turbine performance with tangential synthetic jets located on the intrados and extrados of the airfoil shows an increase in the torque and power output of the turbine. Moreover, using simple estimates, synthetic jets used less power than the increment in power generated at the turbine shaft, showing that efficiency of the turbine increases with the use of synthetic jets. However, the increment in the turbine performance is not as high as in previous two-dimensional studies reported in the literature.

1. Introduction

Energy is essential for human beings and improves people's quality of life. However, the increasing demand for energy, the depletion of fossil fuels, the environmental degradation derived from energy production and climate change require a change in the energy sources, highlighting the use of renewable energies to mitigate these problems. In this field, hydrokinetic energy from rivers and oceans provides a near unexploited alternative with great potential for producing electrical energy. Such energy can be converted into electricity utilizing the so-called hydrokinetic turbines, which mainly are wind turbines adapted to work in an aquatic environment. Consequently, the design optimization of hydrokinetic (HK) turbines is essential for extracting energy from rivers and tidal currents.

HK or water turbines can be classified into two types, depending on how the axis of rotation is oriented concerning the flow direction. There are horizontal axis turbines, in which the rotation axis and the flow direction are parallel, also called Axial Flow Water Turbines (AFWT), and vertical axis turbines, in which the rotation axis and the flow direction are perpendiculars, called Cross-Flow Water Turbines (CFWT). CFWTs allow energy to be extracted independently of the flow direction, this is an important characteristic of these turbines when are compared to AFWTs. However, CFWTs are less efficient than AFWTs because the flow in CFWTs becomes unsteady and is characterized by the shedding of vortices in certain azimuthal positions of the turbine that interact downstream with the blades [1].

To improve CFWT performance, flow control methods have been implemented, allowing the modification of the flow field to reduce the vortex detachment phenomenon. In recent years, flow control techniques have generally focused on controlling boundary layer separation or delay to improve aerodynamic performance. These methods can be classified as passive or active. Passive methods do not require energy to modify the flow and generally correspond to geometric modifications in the airfoil, while active methods require an actuator that consumes energy to modify the flow. Among the passive methods, slats, vortex generators, or gurney flaps are frequently used, and in the active methods, synthetic jets (SJ), plasma actuators, and moving surfaces are the most representative. In particular, SJs modify the flow field by producing changes in the amount of momentum of the boundary layer without introducing a net mass flow to the system; this is achieved by

* Corresponding author.
E-mail address: od.lopez20@uniandes.edu.co (O.D. Lopez Mejia).

https://doi.org/10.1016/j.heliyon.2022.e10017
Received 14 September 2021; Received in revised form 3 April 2022; Accepted 15 July 2022
2405-8440/© 2022 The Author(s). Published by Elsevier Ltd. This is an open access article under the CC BY-NC-ND license (http://creativecommons.org/licenses/by-nc-nd/4.0/).

sucking and expelling the surrounding fluid periodically through an orifice located on the blade's surface [2].

On the other hand, the design of turbines has traditionally been done through experimentation and similarity laws, which are considered expensive processes. Thus, the increase in the processing capacity of computers has allowed the implementation of numerical methods, to design and predict the performance of turbines, making this process cheaper. Computational Fluid Dynamics (CFD) codes have allowed the exploration of the optimal operating conditions for turbines (both for wind or HK applications) by facilitating the integration of different blade profiles [3], geometry modifications [4], different turbine sizes and modification of the tip speed ratio (λ). Mohamed et al. [5] carried out 2D numerical simulations on a Darrieus turbine with straight blades under the sliding mesh approach, using the k-ω SST and Realizable k-ε turbulence models. They studied 25 blade profiles by varying the tip speed ratio between 2 and 9; and tested the performance of the best profile by varying the pitch angle between (−10°, 10°). Results showed that the LS(1)-0413 profile obtained the maximum performance, while the NACA 63-415 profile offers a wider operating range over the tip speed ratio; moreover, they found that a pitch angle of 0° offered the best performance in the LS(1)-0413 profile. Howell et al. [6] conducted a comparative study of the performance of a small vertical axis wind turbine, contrasting experimental wind tunnel data with 2D and 3D simulations. The simulations were carried out under the sliding mesh approach using the k-ε RNG turbulence model. Results showed that the performance coefficient in the 3D simulations was in concordance with the experimental measurements, while 2D simulations showed a significant increase in turbine performance compared to 3D simulations. A similar study was carried out by Siddiqui et al. [7], in which the influence of the geometrical model of a vertical axis turbine on the numerical results was studied. The implemented simulations compared 2D models with complete 3D models, which included the shaft and the supports of the blades. The simulations used the sliding mesh approach and the k-ε Realizable turbulence model. Results showed that 2D simulations could overestimate turbine performance by about 32% compared to 3D simulations, while including shaft and blade supports in 3D simulations can cause a difference of 11 % in the performance calculated concerning the case with only the blades.

CFD has allowed exploration of the optimal configuration of the jet parameters to extract the best performance from the airfoils with SJs as flow control devices. You and Moin [8] implemented Large-Eddy Simulation (LES) on a NACA 0015 profile, studying the effectiveness of synthetic jets as a control method on boundary layer separation. The synthetic jets delayed the flow separation and increased the lift coefficient by approximately 70%. In addition, it was found that both the suction phase and the blowing phase of the jet significantly modify the boundary layer. Zhao et al. [9] carried out a study where the impact of synthetic jets on the dynamic stall in a rotor was evaluated, modifying parameters such as jet location, jet angle, and frequency of actuation, among others. 2D simulations of the airfoil rotor were performed under the Moving-Embedded grids methodology with the k-ω SST turbulence model. According to the study results, synthetic jets achieved the best control over the dynamic stall when they were located near the flow separation point. If jets are located close to the flow separation point, the best control is obtained for small jet angles, while if jets are in the separated flow region, the best control is achieved for medium jet angles. In addition, the control over the actuation frequency showed that the oscillatory suction had the best effect on the control of dynamic stall. Zhu et al. [10, 11] carried out 2D simulations with the sliding mesh approach using the Realizable k-ε turbulence model of a vertical axis turbine when using synthetic jets. In this study, the number of synthetic jets on the profile was varied, and it was found that the aerodynamic performance of the profile is sensitive to the number of jets and that the use of two jets on the trailing edge of the profiles obtained the best performance. In addition, it was observed that power coefficient is reduced with the increment in the momentum coefficient of the jet.

Sasson et al. [12] performed a study based on the single streamtube approach and comparison with experimental data to assess the efficiency of turbines equipped with steady and pulsed synthetic jets versus the bare turbine. As a result, both the power curve and annual energy production are improved in the case of blowing jets. Moreover, the use of synthetic jets helps to alleviate the concern of poor self-starting behaviour of Vertical Axis Wind Turbines (VAWT). Menon et al. [13] employed careful numerical analyses to evaluate the effect of jet operation parameters such as actuator position, reduced frequency or blowing ratio on the 2D aerodynamic performance of the airfoils NACA0018 and DU06-W-200. These authors obtained an increase of 12% in the average axial force over the complete rotation cycle for a blowing ratio of 1.5 and a reduced frequency of 5. Nevertheless, some essential effects were absent in their simulations, such as the effect of finite span blades, spoke drag and wind shear, demanding a full 3D simulation. Yen et al. [14] studied the NACA0020 airfoil model experimentally using synthetic jets at low tip speed ratios (TSR). Their results indicated that such a strategy improves the turbine performance at low TSRs and reduces noise production. However, the study only considered one blade at different angles of attack, which is different from the functional flow conditions of VAWTs.

On the other hand, Maldonado and Gupta [15] experimentally studied the performance of a 3-blades rotor with an S809 airfoil and 60 synthetic jet actuators. At an angular velocity of 500 rpm, the activation of 20 SJs per blade decreases the energy requirement of the rotor by 10.6%, demonstrating that they are a feasible solution for improving the power efficiency of rotors. Wu et al. [16] investigated the effect of synthetic jets control numerically in the energy production of an elliptic airfoil. The airfoil was immersed in a 2D laminar flow, and it experienced an imposed pitching motion combined with a plunging motion. The effects of different parameters, such as inclination angle of the jet, the position of the jet slot, and the phase angle between the jet and the pitching motion on the energy production capability are analized. An increase of up to 30% in energy harvesting can be achieved using synthetic jets in the best configuration. Mohammadi and Maghrebi [17] studied the effect of a jet blowing on the blade suction side of a Horizontal Axis Wind Turbine (HAWT) on the boundary layer separation. 3D Simulations were performed with the software ANSYS Fluent using as turbulence model the k-ω SST model. Different combinations of 2, 3 and 4 jets were investigated versus a single jet, resulting in a direct relation between the number of activated SJs and torque increase. It was found that SJs close to the blade tip were responsible for the highest increase in turbine aerodynamic performance.

The main objective of this study is to present the results of simulations on a straight-bladed Darrieus turbine using synthetic jets as a flow control method. In contrast to other similar studies, in this one, three-dimensional simulations are carried out, and the behaviour of the turbine is studied in water, which allows for reaching higher Reynolds numbers than in air. In addition, a control scheme for the synthetic jets is included to improve their performance on the turbine. The simulation cases are based on the study of Velasco et al. [18], in which two-dimensional simulations were carried out, reproducing the most relevant scenarios to determine the impact of the synthetic jets on the turbine performance in the three-dimensional case compared to the two-dimensional case. The simulations were implemented with the Overset Mesh methodology to capture the dynamic effects of the turbine.

2. Operational parameters of the model

2.1. Hydrodynamic coefficients of the turbine

The non-dimensional parameters that characterize the performance of an HK turbine are:

- Torque coefficient (C_m) which is defined by Eq. (1) and is the dimensionless form of the torque M produced by the turbine

$$C_m = \frac{M}{\frac{1}{2}\rho_\infty U_\infty^2 R S_{ref}} \tag{1}$$

where, ρ_∞ is the density of the fluid, U_∞ is the free-stream velocity, R is the radius of the turbine and S_{ref} is the frontal area of the turbine ($S_{ref} = 2HR$, where H is the span of the blades).

- Power coefficient (C_p) which is defined by Eq. (2) and is the dimensionless form of the power P generated by the turbine.

$$C_p = \frac{P}{\frac{1}{2}\rho_\infty U_\infty^3 S_{ref}} \tag{2}$$

- Normal force coefficient (C_n) defined by Eq. (3) and correspond to the component of the hydrodynamic force applied over the blade that is perpendicular to the chord of the blade profile (F_n). This force component is related to the cyclical structural load applied to the turbine shaft.

$$C_n = \frac{F_n}{\frac{1}{2}\rho_\infty U_\infty^2 S_{ref}} \tag{3}$$

- Tangential force coefficient (C_t) defined by Eq. (4) and correspond to the component of the hydrodynamic force applied over the blades that is parallel to the chord (F_t). This component is responsible for generating torque in the turbine; when this component is in the direction of the rotation of the turbine, it produces energy; otherwise, it consumes energy.

$$C_t = \frac{F_t}{\frac{1}{2}\rho_\infty U_\infty^2 S_{ref}} \tag{4}$$

- Tip speed ratio (λ), defined by Eq. (5) and is the dimensionless form of the angular velocity of the turbine

$$\lambda = \frac{\omega R}{U_\infty} \tag{5}$$

where, ω is the angular velocity.

- The angle of attack (α), defined as the angle between the blade chord and the resultant fluid velocity vector, is given by Eq. (6) [19].

$$\alpha = \tan^{-1}\left[\frac{\sin\theta}{\lambda + \cos\theta}\right] \tag{6}$$

where, θ is the azimuth angle presented in Figure 1.

- Lift (C_L) and drag (C_D) coefficients, which can be obtained from tangential and normal coefficients using the angle of attack as follows in Eqs. (7) and (8).

$$C_L = -C_t \sin\alpha - C_n \cos\alpha \tag{7}$$

$$C_D = C_t \cos\alpha - C_n \sin\alpha \tag{8}$$

2.2. Synthetic jet model

Synthetic jets are zero net mass flow devices, meaning they do not add mass flow to the system. They achieve this with oscillating actuators, which alternate between the suction and expulsion processes of the surrounding fluid. The jets are mainly composed of the vibrator and the cavity. The vibrator is the main component of the jet, that through vibration produces the movement of the fluid from the energy entering the actuator [20]. The vibrator can be a piezoelectric part [21], a piston [22] or a resonant device such as a loudspeaker [23]. However, in this study, the jet cavity is not designed, and instead, the SJs are modelled as a time-dependent inlet/outlet velocity boundary condition, alternating between suction and injection processes. The jet outlet corresponds to a 5 mm (less than 5% of the chord length) wide slot in the blade surface located at 10% of the chord, which corresponds to the same dimensions used in reference [18], on the intrados and on the extrados, as shown in Figure 2. In this model, the neck and the cavity are not included in the computational domain to reduce computational cost.

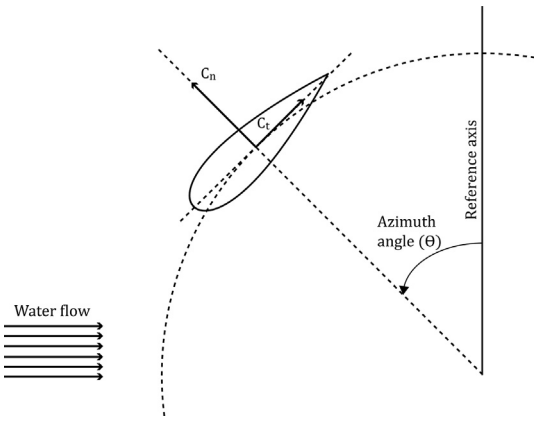

Figure 1. Reference frame of the blades.

The time-dependent velocity boundary condition was implemented as a simple sinusoidal function (see Equation 9), where f_c corresponds to the frequency of actuation of the jet, A is the amplitude, and t is time.

$$V_{jet} = A\sin(2\pi f_c t) \tag{9}$$

Also, the direction of the jet on the profile is specified in the Cartesian system using its components by Eqs. (10) and (11)

$$V_{jet\_x} = A\sin(2\pi f_c t)*\cos(\gamma + \beta + \omega t + \theta_0) \tag{10}$$

$$V_{jet\_y} = A\sin(2\pi f_c t)*\sin(\gamma + \beta + \omega t + \theta_0) \tag{11}$$

where, β is the direction angle for suction/injection of the SJ concerning the jet slot, γ is the angle of the tangent line at the center of the SJ slot and θ_0 is the initial azimuth angle of the location of the SJ slot. In Figure 3, the definition of the angles γ and β is presented.

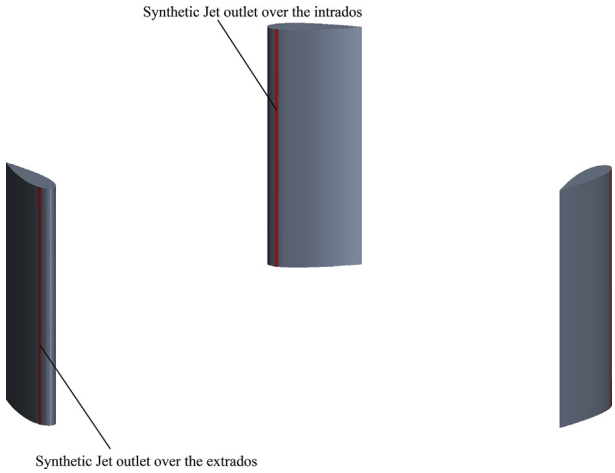

Figure 2. Position of the synthetic jets on the Blades.

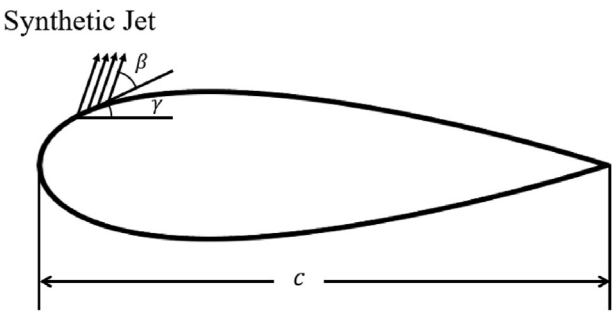

Figure 3. Synthetic jet definition.

Additionally, the most critical operational parameters of the SJs are: the blowing coefficient (C_b), the momentum coefficient (C_μ) and the dimensionless actuation frequency (F^+). These are given by Eqs. (12), (13), and (14), respectively.

$$C_b = \frac{\frac{1}{T}\int_0^{\frac{T}{2}} V_{jet}\, dt}{U_\infty} \tag{12}$$

$$C_\mu = \frac{\frac{1}{T}\int_0^{\frac{T}{2}} \rho_{jet} V_{jet}^2 A_{jet}\, dt}{\frac{1}{2}\rho_\infty U_\infty^2 S_{ref}} \tag{13}$$

$$F^+ = \frac{f_c c}{U_\infty} \tag{14}$$

where, T is the actuation period of the SJ, A_{jet} is the area of the SJ slot, ρ_{jet} is the density of the fluid at the SJ slot (if the fluid is incompressible, as in the present study, $\rho_{jet} = \rho_\infty$), and c is the chord length (see Figure 3).

3. Geometry and mesh

The turbine model analyzed in this work was studied experimentally and computationally by Dai and Lam [24]. It corresponds to a Darrieus straight bladed turbine with a NACA 0025 airfoil; the geometric parameters of the turbine are summarized in Table 1.

Figure 4 present the computational domain used in the simulations, consisting of a rotational domain, where the turbine is located, and a static domain (or background domain) that simulates the free-stream condition. The information transfer between the two domains was carried out using *Overset mesh*, also known as overlapping meshes or chimaera methodology, consisting of independent meshes representing a physical object that exists in the same space with an overlap between them [25]. In *Overset mesh*, near the moving object, the solution is calculated on its mesh; far from it, the solution is also calculated on the background mesh; at the interface between both meshes, the solution is interpolated [25]. The computational domain does not include the blades' supports or the turbine's shaft, as shown in Figure 5. Furthermore, to maintain adequate computational time, only half of the blade span of the blades was simulated, using a symmetry boundary condition. In the rotational domain, each cylinder enclosing the blades has a diameter of 0.9R and a height of 1.1R. Figure 6 shows a Zoom view of the mesh near the synthetic Jet outlet.

Table 1. Geometrical parameters of the turbine.

Parameter	Value
Radius [R]	0.45 m
Reference area [S_{ref}]	0.63 m^2
Chord length [c]	132.75 mm
Number of blades	3
Bladespan [H]	0.7 m
Solidity	0.89

Two meshes were generated for the rotational domain to conduct a convergence analysis, each with a different number and distribution of elements. The most relevant metrics of each mesh are summarized in Table 2. The coarse mesh was built based on reference [1]; for the fine mesh, the density of elements near the walls of each blade was increased.

To guarantee a good overlap of the meshes, the size of the elements must be approximately equal at the interface between the rotating and background meshes. Therefore, two different meshes were generated for the background domain (coarse and fine). It is worth mentioning that the background mesh is entirely structured, as shown in Figure 4. The number of elements of each case used in the convergence analysis is reported in Table 3, and the combination of the rotating and background meshes for convergence analysis is shown in Table 4. The convergence analysis was performed only for the case without actuation, also called the base case.

4. Computational set-up

The simulations were carried out in the commercial software STAR-CCM+ 2019.1.1 V14.02.012. In the analysis, incompressible and isothermal flow is considered, gravitational effects are neglected, and the water is assumed as a Newtonian fluid. Therefore, the governing equations correspond to the averaged mass and momentum conservation equations (Unsteady Reynolds Averaged Navier Stokes or URANS equations) coupled with the k-ω SST turbulence model, while the problem is solved in a transient state, based on the references [1, 18, 24]. Figures 4 and 5 show the boundary conditions in the background and rotational domains, respectively, and Table 5 shows the operational parameters of the simulation. Synthetic jets were implemented at the synthetic jet outlet using a User Defined Function (UDF) following Eqs. (10) and (11). The operational parameters of the SJs were selected according to reference [18], including the amplitude of the SJ, which is $A = 1.5U_\infty$.

Four different cases were studied in the simulations, first, the base case without actuation of the synthetic jets (base case), second, actuation of the synthetic jets on the airfoil extrados; third, actuation of the synthetic jets on the airfoil intrados, fourth, combined actuation of the synthetic jets on the intrados and extrados of the airfoil, using a proposed control approach. For each of these cases, the flow field and results were analyzed after the fifth revolution when the difference between two consecutive cycles was negligible.

5. Results and discussion

5.1. Convergence analysis and base case validation

The convergence analysis and base case validation were performed by comparing the total torque coefficient produced in the three cases shown in Table 4 and its average value with the experimental study carried out by Dai and Lam [24]. Figure 7 shows the evolution of the turbine torque for the three cases used for convergence analysis. The average moment coefficients were 0.139 for case 1, 0.154 for case 2, and 0.155 for case 3. In contrast to the experimental study, the percentage error of each mesh was 11.5%, 1.9%, and 1.2%, respectively. Although case 3 has better results, case 2 had the best compromise between accuracy and computational cost since it took 25% less time than case 3. Thus, it was selected to perform the simulations of the turbine with the synthetic jets. Furthermore, during the simulations, the average wall Y+ was less than 1 for all the cases, which is acceptable.

5.2. Performance of the turbine with synthetic jets

5.2.1. Normal force coefficient (Cn)

Results of the normal force coefficient are presented in Figure 8. When the jet is on the extrados of the blades, it is observed that from an

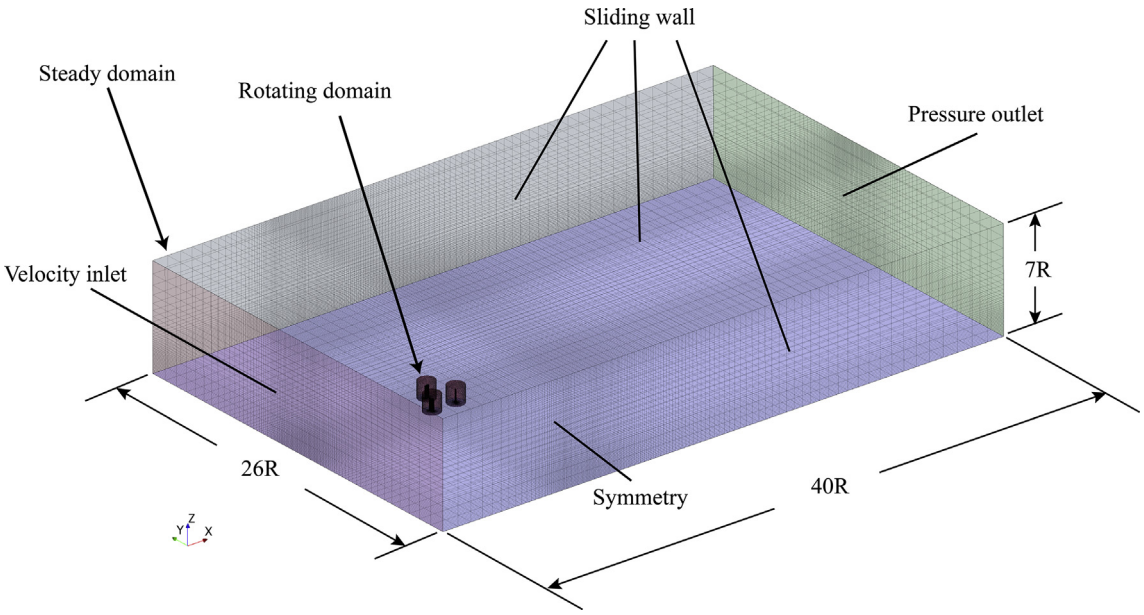

Figure 4. Computational domain and boundary conditions.

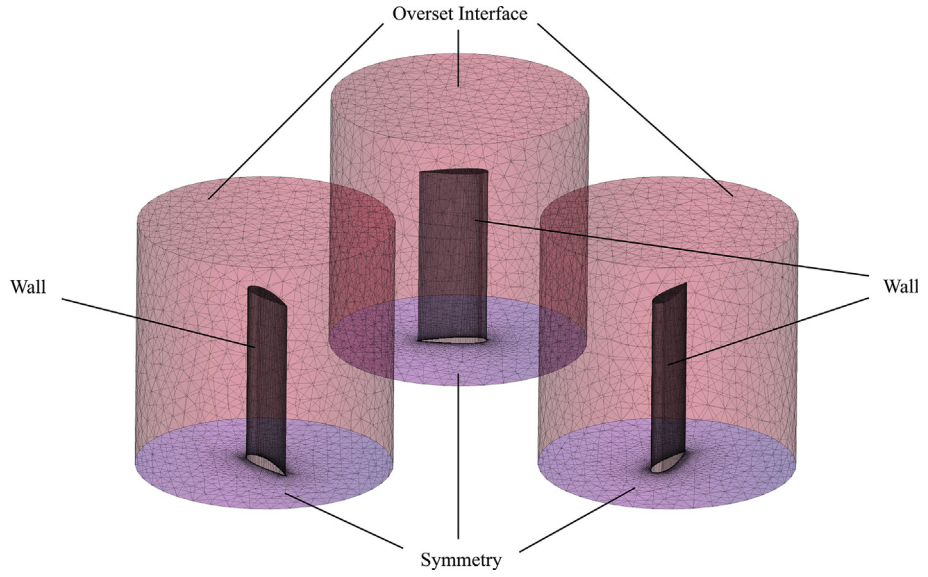

Figure 5. Boundary conditions in the rotational domain.

azimuth angle of 240°, more positive values are obtained until the end of the revolution, in contrast to the base case. When the jet is located on the intrados of the blades, it is observed that Cn remains below the base case curve between 60° and 240°; outside of this interval, Cn remains similar to the base case. It should be noted that the effect of these changes on the coefficient is reflected in a more significant fluctuating load on the turbine shaft. Similar tendencies in the Cn curve have been observed before in both experimental and computational studies [26, 27, 28, 29]. In general, between 0° and 90°, the angle of attack increases so that the lift increases. This lift is the force that contributes to the normal component, as shown in Figure 18. At 90°, the free-stream velocity is perpendicular to the blade chord so that a maximum is achieved in the normal force. Between 90° and 180°, the angle of attack decreases, so the lift force decreases. Downstream the axis of rotation, the evolution of Cn is different due to the influence of the wake of the blades and the shaft. The shed vorticity decreases the effective angle of attack so that the lift generation is affected, and Cn is highly reduced. In theory, an asymmetrical shape was expected for this curve, but the influence of the wake of the blades and the dynamic stall phenomena explain this asymmetry of the Cn curve. The effects of the jet energizing the boundary layer and delaying its separation are represented in the modification of the Cn evolution regarding the base case. For the intrados actuation, the effect is expected in the upstream part of the turbine, in which the jet delays the separation of the leading-edge vortex. On the other hand, for the extrados, the effect is on the downstream part of the turbine since it energizes the boundary layer, reducing the separation zone by moving the separation point towards the trailing edge and increasing the effective angle of attack so that lift is increased as well.

5.2.2. *Tangential force coefficient (Ct)*

Figure 9 presents the results on coefficient of tangential force. It is observed that when the jet is located on the extrados of the blades, the effect of the jet appears close to 180° of azimuth angle until the end of the revolution, obtaining more negative values of the coefficient in contrast

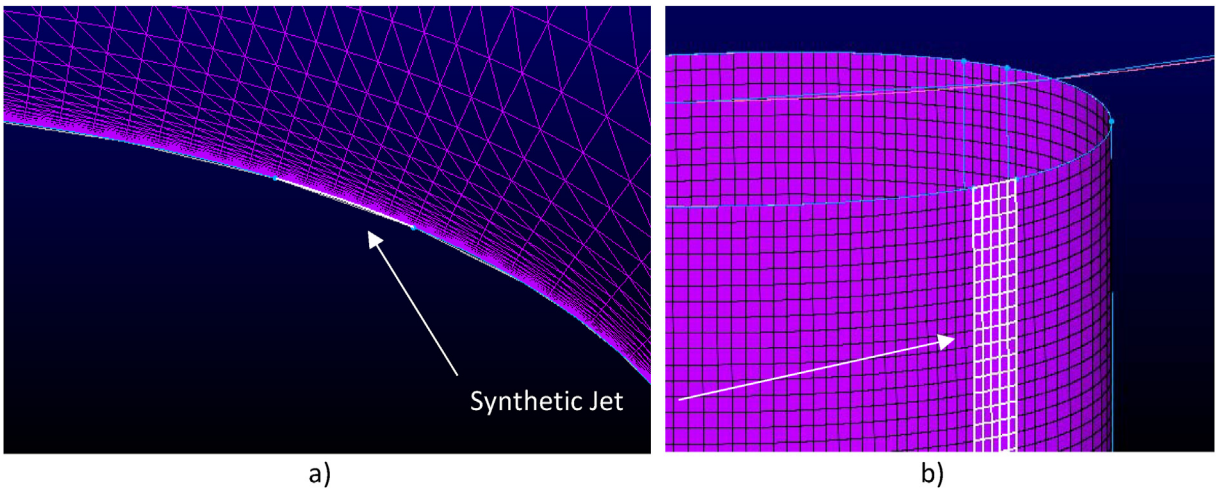

Figure 6. Mesh near the Synthetic Jet outlet. a) Symmetry plane view. b) Surface mesh view.

Table 2. Metrics of Rotational domain meshes.

Metric	Coarse	Fine
Average aspect ratio	253	225
Average skewness equiangle	0.29	0.28
Number of elements	3 519 796	4 635 978

Table 3. Metrics of static (background) domain meshes.

Metric	Coarse	Fine
Average aspect ratio	4.87	2.93
Number of elements	478 170	1 448 370

Table 4. Convergence analysis cases.

Case	Rotating	Background	Total number of elements
1	Coarse	Coarse	3 997 966
2	Fine	Coarse	5 114 148
3	Fine	Fine	6 084 348

Table 5. Computational parameters.

Parameter	Value
Free-stream velocity [U_∞]	1.62 m/s
Turbine Angular Velocity [ω]	60 rpm
Tip speed ratio [λ]	1.745
Blowing coefficient [C_b]	0.48
Momentum coefficient [C_μ]	6.25×10^{-3}
Non-dimensional actuation frequency [F^+]	4.1
Jet suction/injection angle [β]	0°
Iterations per time step	40
Time step without actuation of the jets	0.005 s
Time step with actuation of the jets	0.002 s
Fluid	Water @ 20 °C
Time discretization order	Second
Spatial discretización order	Second
Type of coupling	Segregated
Coupling scheme	SIMPLE

to the base case, consequently, in this interval, there is an increase of the power generated in the turbine shaft. When the jet is located on the intrados, the coefficient curve shows more negative values than the base case curve in an interval between 60° and 180°, in which greater power is generated in the turbine than in the base case. However, between 180° and 240°, Ct shows fewer negative values; thus, the power generation decreases in this interval compared to the base case. Similar to the normal force, the behaviour of the tangential force has been reported previously in the [30, 31, 32]. The tangential force is highly influenced by the lift that increases between 0° and 90° (reaching its maximum) due to the increment of the angle of attack. As the blade rotates from 90° to 180°, the lift reduces and a leading-edge vortex is formed, affecting the pressure distribution. In the downstream part of the turbine, there is also a strong influence of the wake of the blades and the turbine's shaft, reducing the lift and the tangential force. The same aspects analyzed in section 5.2.1 explain the differences between actuation and base cases. This will be discussed later in sections 5 and 5.6.

5.2.3. *Torque coefficient (Cm) on one blade*

Since the torque is proportional to the tangential force because T = Ft*r, the curves of the torque coefficient retain the same behaviour of the tangential force coefficient described in section 5.2.2 but are inverted (see Figure 10), thus, with the jets on the extrados, an increase in the torque coefficient is observed from 180° until the end of the turn, and with the jets on the intrados, an increase in the torque coefficient between 60° and 180° is observed, as suggested by the curves of the tangential force coefficient.

5.2.4. *Total torque coefficient (Cm)*

Figure 11 shows the results of the total torque coefficient, in which it is clear that the curves of the base case and the jets on the extrados do not have a negative component. Besides, with the actuation on the extrados, an average total torque coefficient of 0.167 is achieved, increasing the average torque generated in the turbine by 8.4%. Meanwhile, with the action of the jets on the intrados, an average total torque coefficient of 0.208 is achieved, increasing the average torque generated in the turbine by 35.1%. Additionally, the average power generated in the turbine in the base case was 359 W, in the case of the jets on the extrados 389 W and with the jets on the intrados 485 W. It should be noted that a simple estimation of the average power consumption of the jets shows that it is approximately 11 W; thus, it is shown that the generation of power due to the jets is more significant than their power consumption, increasing the net efficiency of the turbine. In the turbine, the generation of torque or net power is more significant than zero because the net torque is the sum of the contributions of each of the blades; thus, while some of the blades

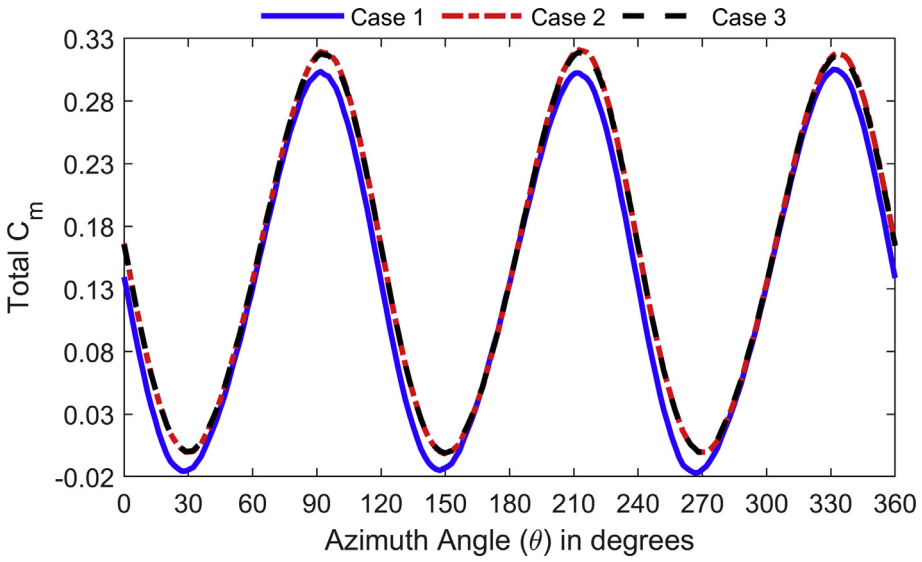

Figure 7. Total torque coefficient during one revolution of the turbine for each convergence case.

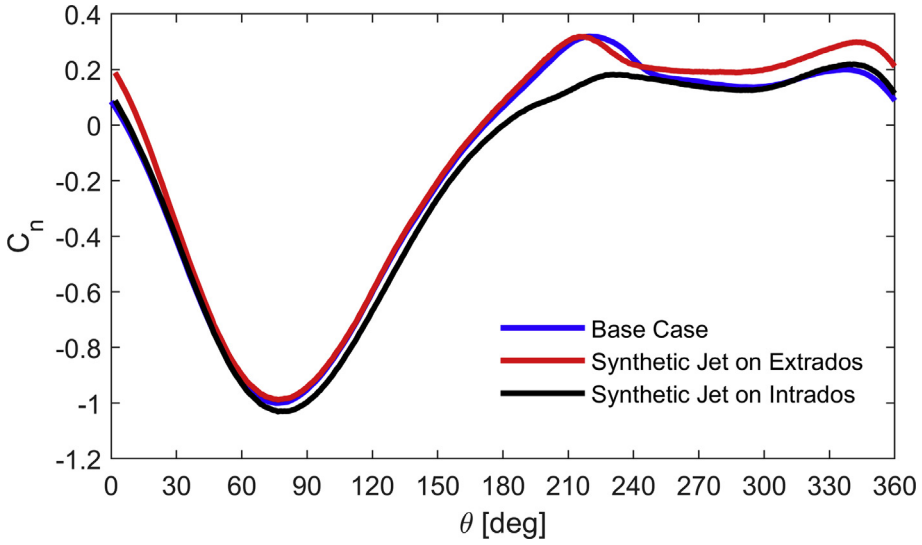

Figure 8. Normal force coefficient for a blade during one revolution of the turbine.

consume power, the others compensate for it, obtaining a net power generation greater than zero, which is why the peaks are repeated three times in each revolution when each blade is passing through the upstream zone.

5.3. Performance of a proposed control system

From the results of the torque coefficient on a blade, a control system was designed for alternating actuations between the jets on the intrados and the jets on the extrados during one revolution of the turbine, shown in Figure 12. The proposed system works as follows: between 0° and 60°, there is no actuation of the jets; between 60° and 180°, the jets are active on the intrados, and between 180° and 360°, the jets are active on the extrados. Figure 13 shows the behaviour of the torque coefficient when the control system is active; as it can be seen; the control system combines the best characteristics of both types of actuations to improve power generation between 60° and 180° with the use of the jets on the intrados, and improving power generation between 180° and 360° with the use of the jets on the extrados.

Figure 14 shows the coefficient of total torque of the control system in contrast to the previous cases. The behaviour of the control system is similar to the curve of the jets on the intrados, with the difference that it reaches a maximum in the curve similar to the curve with jets on the extrados. On the other hand, the average coefficient of total torque in the control system is equal to 0.211, an increase of 37% concerning the base case; in addition, the average power generated was 492 W.

5.4. Comparison with two-dimensional simulations

The comparison was made using the average torque coefficients reported in reference [18]; this information is presented in Table 6. It is clear that in 2D simulations, the hydrodynamic coefficient had a greater magnitude; this is because, in the 2D simulations, the effect of the vortices at the tip of the blades is neglected, which is in agreement with the results found by Howell et al. [6]. On the other hand, it is found that

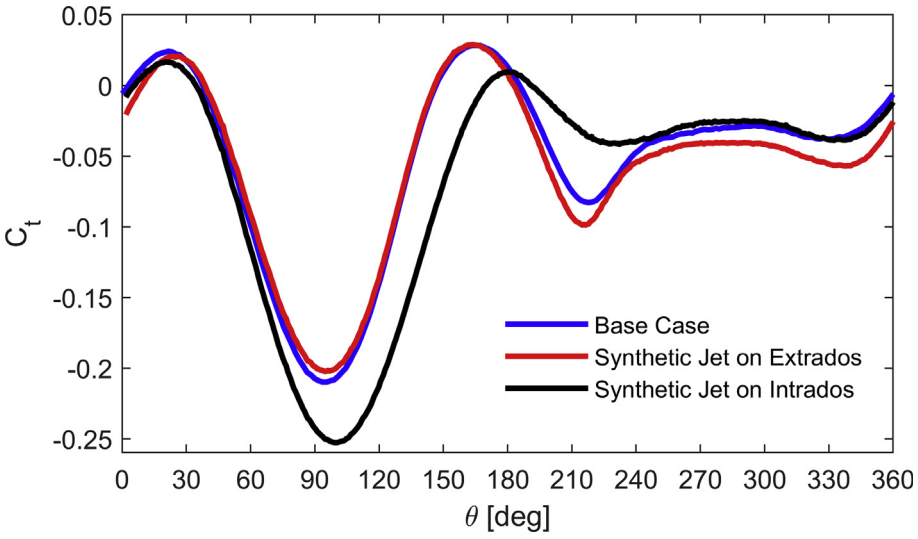

Figure 9. Tangential force coefficient for a blade during one revolution of the turbine.

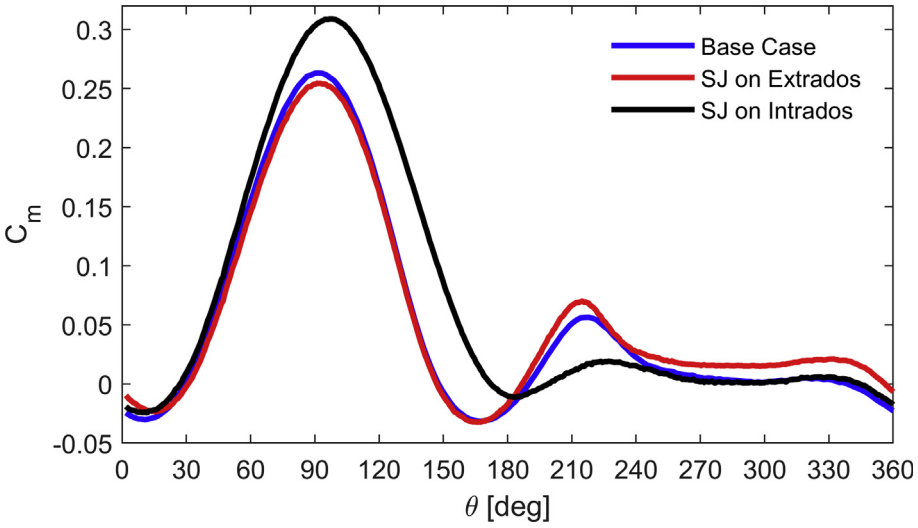

Figure 10. Torque coefficient for a blade during one revolution of the turbine.

the effect of the jets on the extrados of the profile is reduced in the 3D case since the increase of the coefficient in the 2D simulations was 41.7%, while in the 3D simulations, it was only 8.4%. With the simulations on the intrados, it is observed that there was a significant increase in the coefficient in both cases, being 45.8% in the 2D simulations and 35.1% in the 3D simulations. Moreover, it is observed that, in both cases, the control system obtained the best performance, with the most significant increase in the coefficient, but due to the reduction in the effect of the jets on the extrados in the 3D case, the increase in the coefficient in the case 3D was only 37% (just 1.4% higher than the case with jets on the intrados), while in the 2D case it was 81.5%.

5.5. Vorticity field and vortical structures visualization

Figure 15 shows the instantaneous vorticity field near the turbine with an azimuth angle of 30° in planes at different positions along the blade span of the blades, which correspond to half the blade span (z = 0 m), a quarter blade span (z = 0.175 m) and the tip of the blade (z = 0.35 m). Furthermore, to analyze the effects of the synthetic jets, three positions have been defined in the turbine blades, position one (B1) is equivalent to an azimuth angle of 30°, position two (B2) to an azimuth angle of 150°, and position three (B3) to an azimuth angle of 270°.

In Figure 15-a, it can be seen that in the base case, when blade 1 moves to the position of blade 2, a large vortex is generated on the intrados of the blade. Then, when blade 2 moves to the position of blade 3, it is observed that the large vortex detaches from the blade, corresponds to the *Omega vortex* (see Figure 16-b), and is highlighted by the red circle. Moreover, a large vortex is generated on blade 3 near the trailing edge on the side of the extrados. In the controlled case, it can be observed that on blade 2, the size and strength of the vortex decreased due to the action of the jets in the intrados, which operate between the position of blade 1 and blade 2. In addition, the *Omega vortex* moved slightly downwards, avoiding the crossing with the blades during the revolutions of the turbine, and on blade 3, the size of the vortex that was

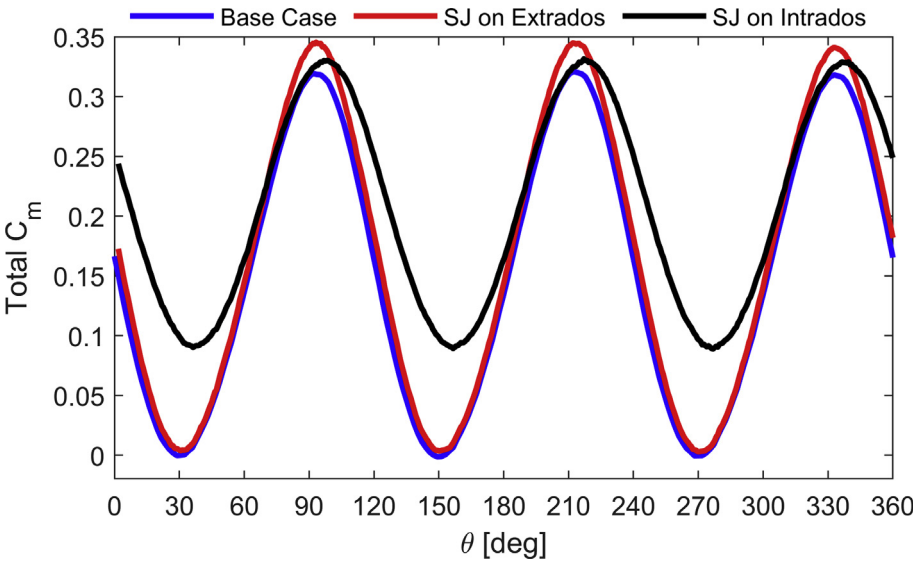

Figure 11. Total torque coefficient during one revolution of the turbine.

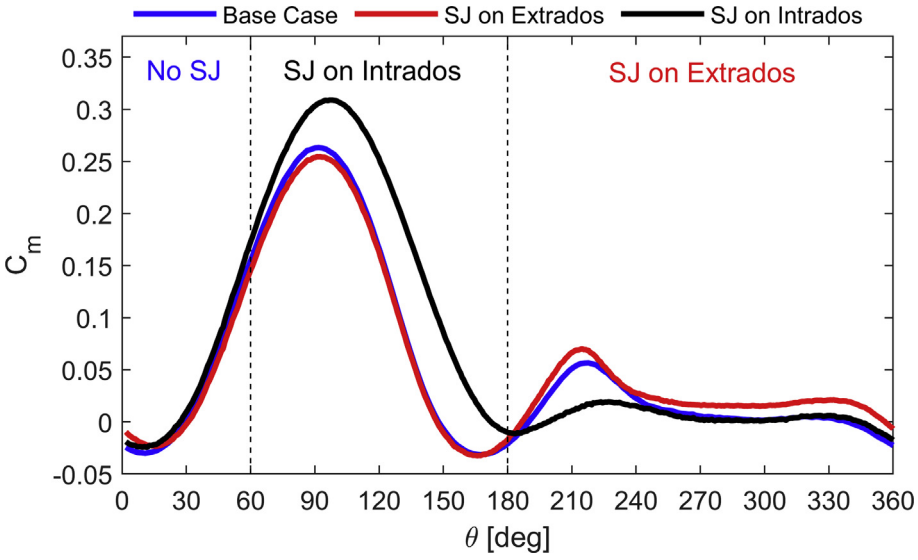

Figure 12. Definition of the control system.

located at the trailing edge was reduced to the action of the jets on the extrados.

In Figure 15-b, with the plane over a quarter of the blade span, it can be observed that the vorticity behaviour is very similar to that shown in Figure 15-a over the central plane of the turbine. The main difference between these two planes is the size and strength of the vortices around the blades, which decreases.

In Figure 15-c on the tip of the blades, different behaviour of vorticity is observed compared to Figure 16-a and 16-b, but there are no significant differences between the base case and the control system since the vortices formed in this plane are due to the interaction between the fluid and the tip of the blades, which are the same in both cases, and the influences of the SJs are negligible.

Figure 16 shows the structure of the vortices between 0° and 60° azimuth angle, and these vortices are defined using the Q-criterion with a value of 30 s^{-2} (In Figure 16, it is essential to mention that the flow direction goes from left to right). The main difference between the case with the control system and the base case occurs in the area enclosed by the red circle, where there is a reduction in the size of the highlighted vortex, and there is a faster separation of the vortex and the blade. The jets' action is to separate this vortex from the blade and reduce its interaction with the tip vortex. This vortex, known as the *Omega vortex*, was previously studied by Lain et al. [1] and is closely related to the dynamic stall phenomenon in CFWT's. Omega vortex is generated in the intrados of the blades when they sweep 180° of azimuth angle, which can be observed by looking at the progression of blades 1 and 2 in Figure 16; thus, the reduction in its size is due to the effect of the jets on the intrados of the blades that are activated between 60° and 180° of azimuth angle, delaying the formation and separation of this vortex. On the other hand, the vortex enclosed by the black circle, which is formed at the tip of the blades, is responsible for decreasing the magnitude of the hydrodynamic coefficients when moving from 2D simulations to 3D simulations.

From the analysis made previously, it is observed that the increase in the torque coefficient due to the effect of the jets on the intrados, is that it

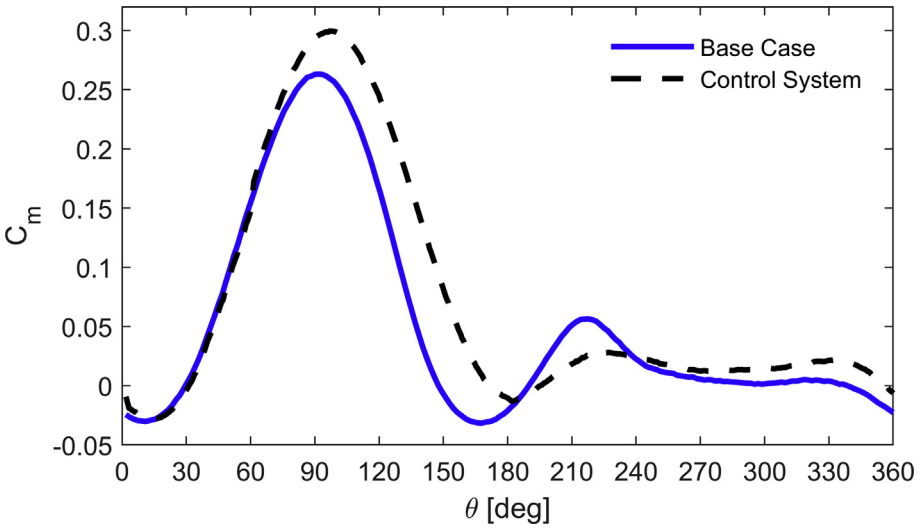

Figure 13. Torque coefficient on the control system.

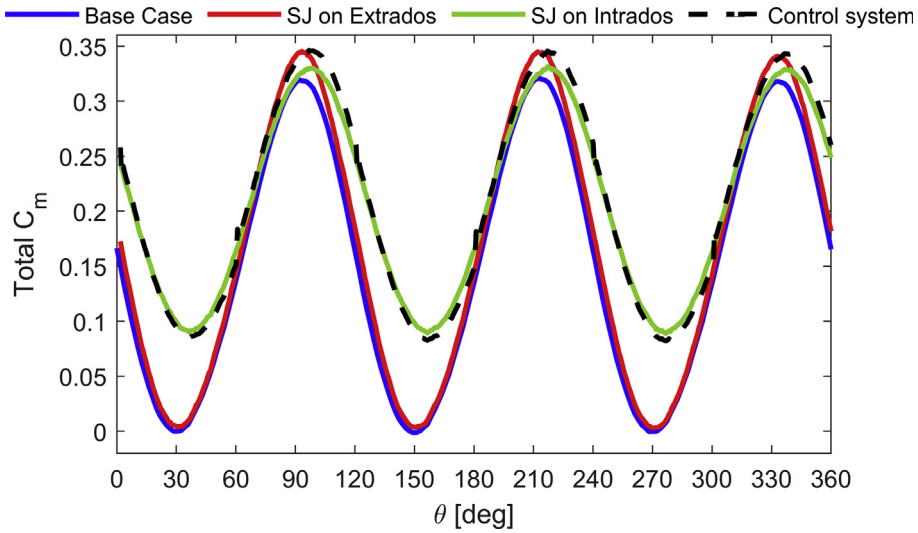

Figure 14. Comparison of the total torque coefficient of all cases.

Table 6. Comparison of average torque coefficient of 2D and 3D simulations. Data from ref [21].

Study case	Two-dimensional	Three-dimensional
Base case	0.168	0.154
SJ on Extrados	0.238	0.167
SJ on Intrados	0.245	0.208
Control System	0.305	0.211

delays the formation of the omega vortex inside the blade between 60° and 180° of the azimuthal angle while it promotes its separation from the blade. In the same way, the increase in the torque coefficient due to the effect of the jets on the extrados is owing to the delay in the formation of the vortex at the blade trailing edge between the angles of 180° and 360°.

5.6. Dynamic stall analysis

The dynamic stall analysis was performed by visualizing the evolution of the drag, lift, and torque coefficients concerning the angle of attack (see Figure 17). The first observation is that upstream, the dynamic stall occurs near $\alpha = 26°$ ($\theta = 76°$). The second observation is the differences found between the simulated cases; for example, on the drag coefficient plot, it is observed that between $35° > \alpha > 5°$ ($124° > \theta > 176°$), after the dynamic stall occurs, the curves of the control system and the jets on the intrados show a decrease in the value of the coefficient concerning the base case. On the downstream section, between $-20° > \alpha > -35°$ ($196° < \theta < 235°$), the curves of the base case and the jets on the extrados present the highest magnitudes in the coefficient and during the recovery of the dynamic stall between $-12° < \alpha < 5°$ ($326° < \theta < 360°$, $0° < \theta < 14°$) the curves of the control system and the jets on the extrados show an increase in the magnitude of the coefficient tending to more negative values.

Regarding the plot of the lift coefficient, it is observed that, after the dynamic stall, between $35° > \alpha > -35°$ ($124° < \theta < 235°$), the curves of the control system and the jets on the intrados remain above of the curves of the base case and the jets on the extrados. Furthermore, during dynamic stall recovery, between $-35° < \alpha < 10°$ ($235° < \theta < 360°$, $0° < \theta < 29°$), the curves of the control system and the jets on the extrados remain below the base case curves and jets on the intrados.

Regarding the torque coefficient, it is observed, in the upstream region, an increase in the value of the coefficient in the curves of the

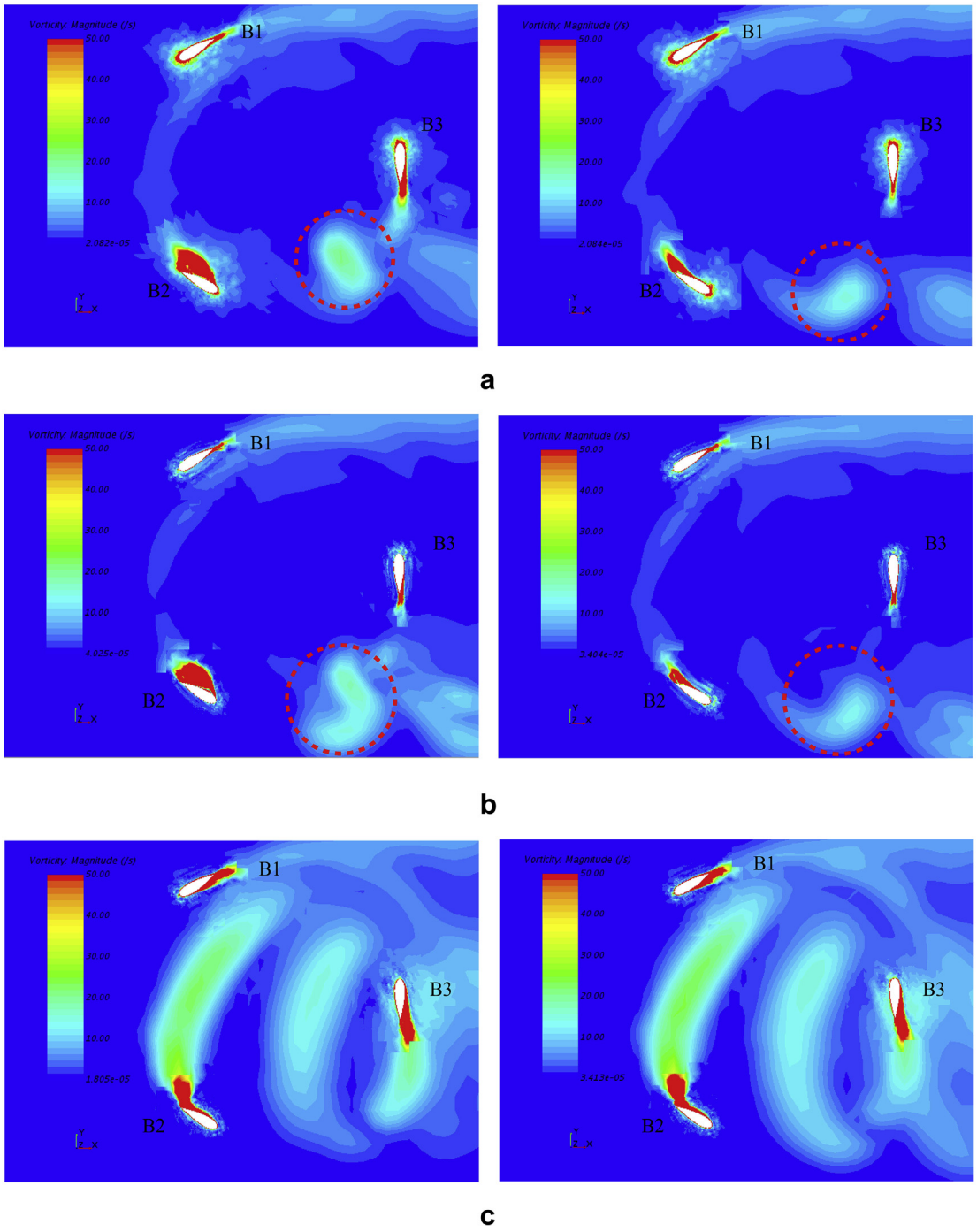

Figure 15. Comparison of vorticity fields between base case (left) and control system (right). a) z = 0 m, b) z = 0.175 m and c) z = 0.35 m.

control system and the jets on the intrados, which occurs before the dynamic stall and is maintained after the dynamic stall until the downstream region begins. Over the downstream region, the base case curves and the jets on the extrados remain above the curves of the control system, and the jets on the intrados between $0° > \alpha > -35°$ ($180° < \theta < 235°$).

Moreover, in Figure 18, the drag and lift coefficients are compared at different azimuthal positions for the base case and the control system (the size of the vectors is proportional to the magnitude). As can be seen in the upstream region, at $\theta = 45°$, before the jets on the intrados are activated, the magnitude of the drag and lift coefficients are approximately equal in both cases. At $\theta = 135°$, with the jets on the intrados activated, the lift coefficient presents an increase in its magnitude while the drag coefficient decreases. In the downstream region, at $\theta = 225°$, during the transition between the effect of the jets on the intrados to the jets on the extrados, the lift and drag coefficients decrease in magnitude compared to the base case. After the effect of the jets on the extrados has been established, at $\theta = 315°$, the lift coefficient increases in magnitude compared to the base case, and the drag coefficient remains approximately equal in both cases.

From the analysis of Figure 18, it can be concluded that the synthetic jets increase the lift coefficient of the blades in the downstream and upstream regions, generating a net increment in the power produced by the turbine.

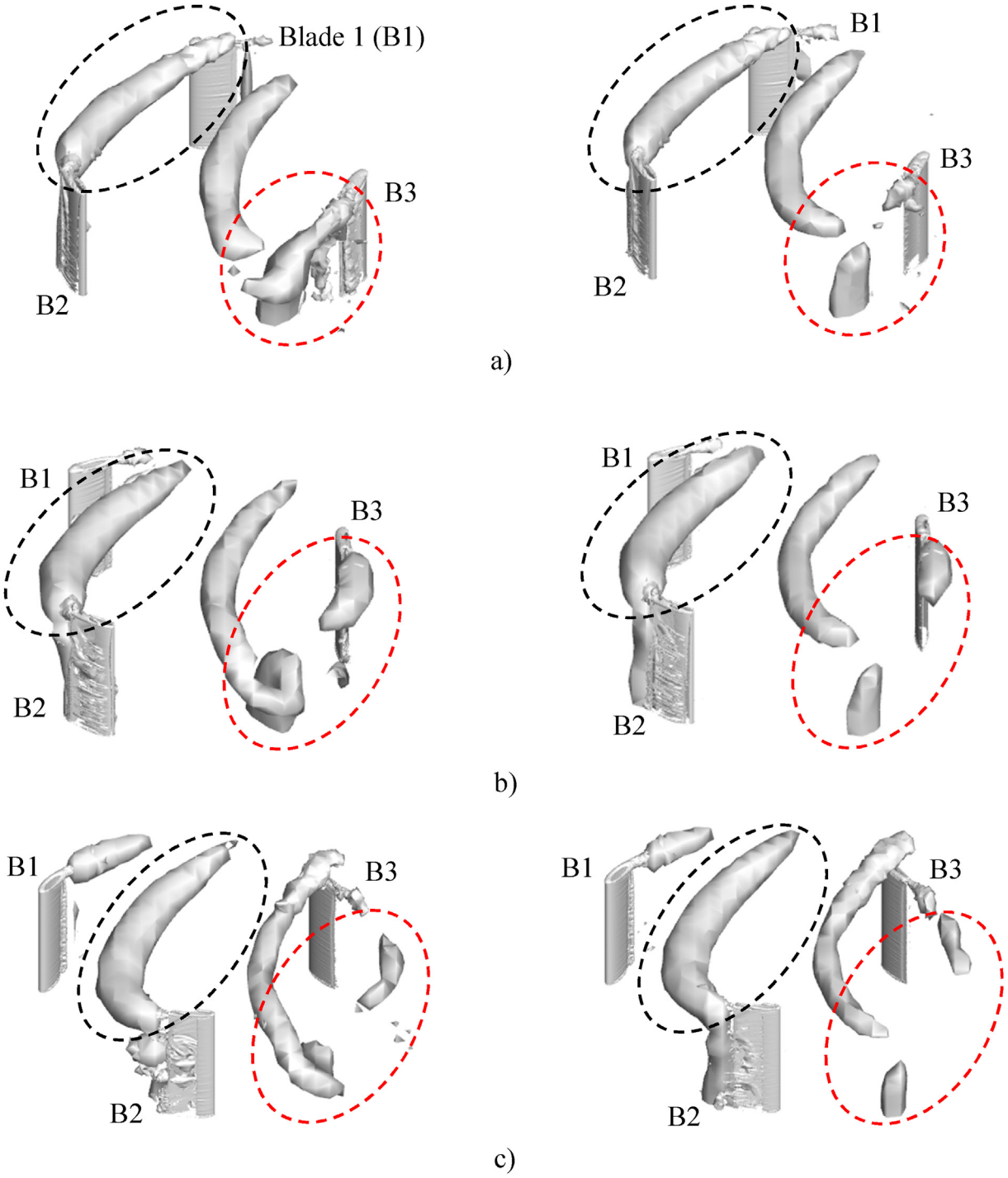

Figure 16. Comparison of vortical structures using Q-Criterion between base case (left) and control system (right). a) $\theta = 0°$, b) $\theta = 30°$ and c) $\theta = 60°$.

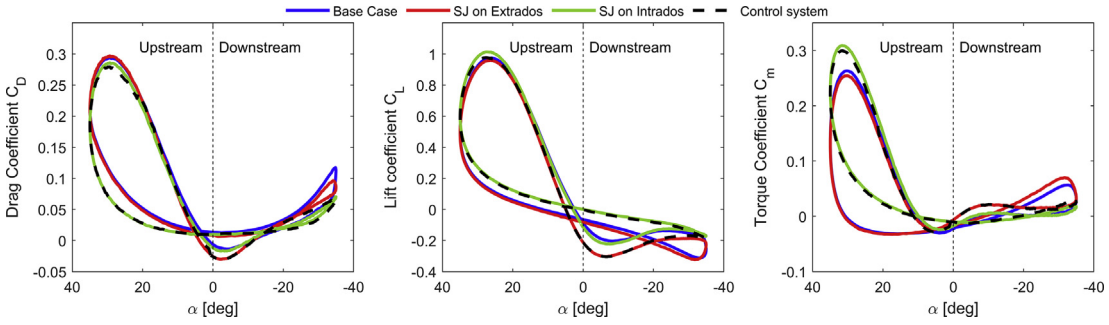

Figure 17. A blade's drag, lift, and torque coefficient during one turbine revolution. a) drag coefficient, b) lift coefficient, c) Torque coefficient

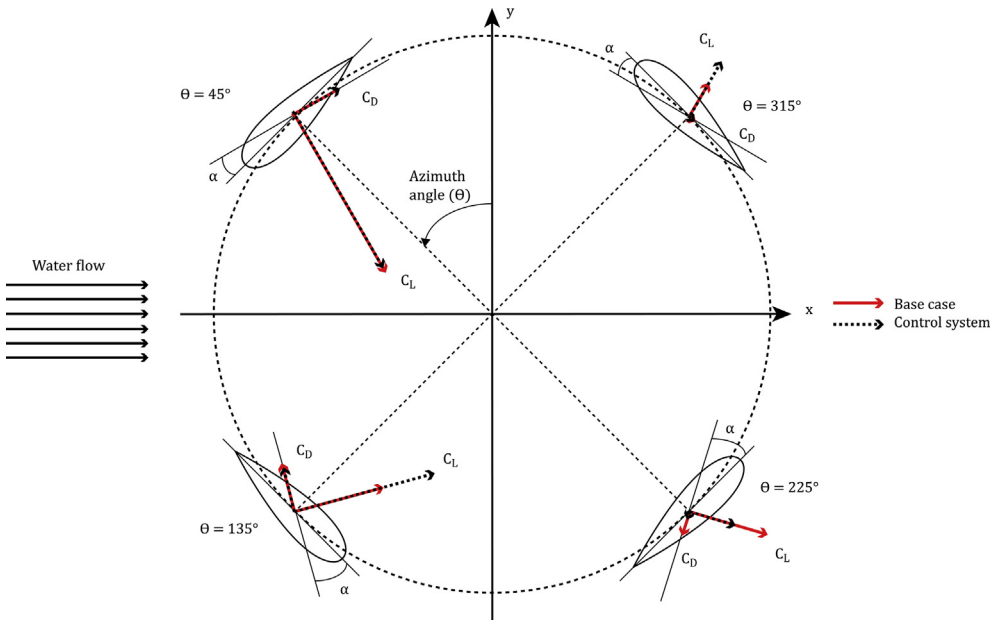

Figure 18. Comparison of the drag and lift coefficients vectors between the base case and the control system at different azimuthal positions.

6. Conclusions

Through a systematic convergence analysis and the validation of the base case, it was determined that Case 2 (a combination of a fine grid in the rotating domain with a coarse-size mesh in the background) achieves the best results with an acceptable computational cost. Thus, the average torque coefficient obtained has a percentage error of 1.9% compared to the experimental results of Dai and Lam [24].

The simulation with the SJ on the extrados showed a more significant torque generation from an azimuth angle of 180°–360° for one blade. At the same time, simulation with the SJ on the intrados showed a more significant generation of torque from an azimuth angle of 60°–180°. In addition, on the total torque coefficient, on the SJ on extrados, a greater amplitude is obtained in the coefficient curve and an increase in the average coefficient of 8.4% over the base case; while, on the SJ on intrados, a lower amplitude of the curve is obtained and an increase in the average of the coefficient of 35.1% over the base case. The control system demonstrated the best performance and the most significant increase in torque and power generated in the turbine. The increase in the average torque due to the control system was 37% over the base case, 1.4% greater than the case of the jets on the intrados and 26.3% greater than the case of the jets on the extrados.

In contrast to the 2D simulations of Velasco et al. [18], for any type of action of the jets, there was a reduction in the magnitude of the hydrodynamic coefficients due to the vortex formation at the tip of the blades. In the 3D case, the improvement in the total moment coefficient over the base case for the jets in the extrados, intrados, and control system was 8.4%, 35.1%, and 37%, respectively. Meanwhile, in the 2D case, it was 41.7%, 45.8%, and 81.5%, respectively, for the same configurations of the jets. Therefore, it is observed that the effect of the jets on the extrados decreases its impact in the 3D case.

The jets on the intrados delay the formation and separation of a vortex inside the blades that are generated between 0° and 180° of rotation of the azimuth angle, which is reflected in the increase of the torque coefficient on a blade between 60° and 180° for the configuration of the jets on the intrados. The jets on the extrados delay the formation of a vortex on the outer face of the blade, near the trailing edge, between 180° and 360°, an effect that is reflected in the increase of the torque coefficient on a blade between 180° and 360° for the configuration of the jets on the extrados.

From the dynamic stall analysis, the jets on the intrados improve turbine performance by increasing the lift coefficient in the upstream region, while the jets on the extrados improve the turbine performance by increasing the magnitude of lift coefficient in the downstream region.

Finally, the improvements presented in the turbine's performance due to the synthetic jets offer an advantageous alternative to improve the efficiency of this type of turbine in the extraction of hydrokinetic energy and promote their implementation in renewable energies.

Declarations

Author contribution statement

Nicolas Botero: Conceived and designed the experiments; Performed the experiments; Analyzed and interpreted the data; Wrote the paper.

Nicolas Ratkovich, Santiago Lain: Contributed reagents, materials, analysis tools or data; Wrote the paper.

Omar D Lopez Mejia: Conceived and designed the experiments; Analyzed and interpreted the data; Contributed reagents, materials, analysis tools or data; Wrote the paper.

Funding statement

This work was supported by the mechanical engineering department and the Vice-Presidency for Research & Creation at Universidad de los Andes.

Data availability statement

Data included in article/supplementary material/referenced in article.

Declaration of interests statement

The authors declare no conflict of interest.

Additional information

No additional information is available for this paper.

Acknowledgements

The authors acknowledge the mechanical engineering department at Universidad de los Andes for providing the computational resources for this study.

References

[1] S. Laín, P. Cortés, O.D. López, Numerical simulation of the flow around a straight blade Darrieus water turbine, Energies 13 (5) (2020) 1137.
[2] K. Mohseni, R. Mittal, Synthetic Jets: Fundamentals and Applications, CRC Press Taylor & Francis Groups, Boca Raton, 2014.
[3] X. Sun, J. Zhu, A. Hanif, Z. Li, G. Sun, Effects of blade shape and its corresponding moment of inertia on self-starting and power extraction performance of the novel bowl-shaped floating straight-bladed vertical axis wind turbine, Sustain. Energy Technol. Assess. 38 (2020), 100648.
[4] M.Y. Roshan, J. Khaleghinia, M.E. Nimvari, H. Salarian, Performance improvement of Darrieus wind turbine using different cavity layouts, Energy Convers. Manag. 246 (2021), 114693.
[5] M. Mohamed, A. Ali, A. Hafiz, CFD analysis for H-rotor Darrieus turbine as a low speed wind energy converter, Eng. Sci. Technol. Int. J. 18 (2015) 1–13.
[6] R. Howell, N. Qin, J. Edwards, N. Durrani, Wind tunnel and numerical study of a small vertical axis wind turbine, Renew. Energy 35 (2010) 412–422.
[7] M.S. Siddiqui, N. Durrani, I. Akhtar, Quantification of the effects of geometric approximations on the performance of a vertical axis wind turbine, Renew. Energy 74 (2015) 661–670.
[8] D. You, P. Moin, Active control of flow separation over an airfoil using synthetic jets, J. Fluid Struct. 24 (2008) 1349–1357.
[9] Q. Zhao, Y. Ma, G. Zhao, Parametric analyses on dynamic stall control of rotor airfoil via synthetic jet, Chin. J. Aeronaut. 30 (2017) 1818–1834.
[10] H. Zhu, W. Hao, C. Li, Q. Ding, Simulation on flow control strategy of synthetic jet in an vertical axis wind turbine, Aero. Sci. Technol. 77 (2018) 439–448.
[11] H. Zhu, W. Hao, C. Li, Q. Ding, B. Wu, Application of flow control strategy of blowing, synthetic and plasma jet actuators in vertical axis wind turbines, Aero. Sci. Technol. 88 (2019) 468–480.
[12] B. Sasson, D. Greenblatt, Effect of Steady an Unsteady Slot Blowing on a Vertical Axis Wind Turbine, 28th AIAA Applied Aerodynamics Conference, 2010.
[13] A. Menon, Numerical Investigation of Synthetic Jet Based Flow Control for Vertical axis Wind Turbines, Rensselaer Polytechnic Institute, 2014.
[14] J. Yen, N.A. Ahmed, Enhancing vertical axis wind turbine by dynamic stall control using synthetic jets, J. Wind Eng. Ind. Aerod. 114 (2013) 12–17.
[15] V. Maldonado, S. Gupta, Increasing the power efficiency of rotors at transitional Reynolds numbers with synthetic jet actuators, Exp. Therm. Fluid Sci. 105 (2019) 356–366.
[16] J. Wu, M. Shen, L. Jiang, Role of synthetic jet control in energy harvesting capability of a semiactive flapping airfoil, Energy 208 (2020), 118389.
[17] M. Mohammadi, M.J. Maghrebi, Improvement of wind turbine aerodynamic performance by vanquishing stall with active multi air jet blowing, Energy 224 (2021), 120176.
[18] D. Velasco, O. López, S. Laín, Numerical simulations of active flow control with synthetic jets in a Darrieus turbine, Renew. Energy 113 (2017) 129–140.
[19] S. Roy, H. Branger, C. Luneau, D. Bourras, B. Paillard, DESIGN of an offshore three-bladed vertical axis wind turbine for wind tunnel experiments, Ocean Renew. Energy 10 (2017).
[20] P. Wang, Q. Liu, C. Li, W. Miao, S. Luo, K. Sun, K. Niu, Effect of trailing edge dual synthesis jets actuator on aerodynamic characteristics of a straight-bladed vertical axis wind turbine, Energy 238 (2021), 121792.
[21] R. Rimasauskiene, M. Matejka, W. Ostachowics, M. Kurowski, P. Malinowski, T. Wandowski, M. Rimasauskas, Experimental Research of the Synthetic Jet Generator Designs Based on Actuation of Diaphragm with Piezoelectric Actuator, Mechanical Systems and Signal Processing, 2014, pp. 607–614.
[22] Y.-W. Lyu, J.-Z. Zhang, C. Tang, X.-m. Tan, Temperature-variation effect of piston-driven synthetic jet and its influence on definition of heat transfer coefficient, Int. J. Heat Mass Transfer 152 (2020), 119347.
[23] M. Zaccara, G. Paolillo, C.S. Greco, T. Astarita, G. Cardone, Flow control of wingtip vortices through synthetic jets, Exp. Therm. Fluid Sci. 130 (2022), 110489.
[24] Y.M. Dai, W.-H. Lam, Numerical study of straight-bladed Darrieus-type tidal turbine, Proceed.e Instit. Civ. Eng. - Energy 162 (2009) 67–76.
[25] J.L. Steger, F. Dougherty, J.A. Benet, A Chimera Grid Scheme vol. 5, American Society of Mechanical Engineers, Fluids Engineering Division (Publication) FED, 1983.
[26] E. Dyachuk, M. Rossander, A. Goude, H. Bernhoff, Measurements of the aerodynamic normal forces on a 12-kW straight-bladed vertical Axis wind turbine, Energies 8 (2015) 8482–8496.
[27] M. Nguyen, F. Balduzzi, A. Goude, Effect of pitch angle on power and hydrodynamics of a vertical axis turbine, Ocean Eng. 238 (2021).
[28] F. Scheurich, T. Fletcher, R. Brown, Effect of blade geometry on the aerodynamic loads produced by vertical-axis wind turbines, Proc. Inst. Mech. Eng. Part A Journal of Power and Energy 225 (3) (2011) 327–341.
[29] F. Scheurich, T. Fletcher, R. Brown, Simulating the aerodynamic performance and wake dynamics of a vertical-axis wind turbine, Wind Energy 14 (2011) 159–177.
[30] K. McLaren, S. Tullis, S. Ziada, Computational fluid dynamics simulation of the aerodynamics of a high solidity, small-scale vertical axis wind turbine, Wind Energy 15 (2012) 349–361.
[31] K. Wang, M. Hansen, T. Moan, Model improvements for evaluating the effect of tower tilting on the aerodynamics of a vertical axis wind turbine, Wind Energy 18 (2015) 91–110.
[32] Q. Liu, W. Miao, C. Li, W. Hao, H. Zhu, Y. Deng, Effects of trailing-edge movable flap on aerodynamic performance and noise characteristics of VAWT, Energy (2019), 116271.